Influence of cobalt doping on the structural, optical, and magnetic properties of hydrothermally prepared $NiMnO_3$ perovskite oxides

B. Mahalakshmi [a], L. Balakrishnan [b,*], S. Esakki Muthu [c,d], J. Thirupathy [e]
[a] *Department of Physics, Hindusthan College of Engineering and Technology, Coimbatore, India-641021*
[b] *Department of Physics, Government College of Technology, Coimbatore - 641 013, India*
[c] *Centre for Materials Science, Karpagam Academy of Higher Education, Coimbatore, India-641 021*
[d] *Department of Physics, Faculty of Arts Science Commerce and Management, Karpagam Academy of Higher Education, Coimbatore, India-641 021*
[e] *Department of Physics, Saveetha Engineering College,Thandalam,Chennai - 602105*

$NiMnO_3$, a perovskite oxide, is renowned for its exceptional physical and chemical characteristics, affordability, and non-toxicity. In this work, we investigate how cobalt (Co) doping affects the optical, magnetic, and structural characteristics of $NiMnO_3$ nanoparticles made using the hydrothermal method. Powder X-ray diffraction (XRD), UV-visible spectroscopy, photoluminescence (PL) spectroscopy, scanning electron microscopy (SEM), and vibrating sample magnetometry (VSM) were used to evaluate the produced $NiMnO_3$, $NiMn_{0.95}Co_{0.05}O_3$,and $NiMn_{0.9}Co_{0.0}O_3$nanoparticles. XRD analysis confirm the rhombohedral crystal structure with a minor shift in peaks indicating successful doping of Co. UV-Vis spectroscopy revealed a decrease in bandgap with increasing Co concentration, while PL analysis showed a reduction in near band edge and increase in emission intensity, defect level transitions. SEM images highlighted a change in morphology and particle size with higher Co doping. Magnetic studies demonstrated an increase in coercive field with Co content, indicating enhanced magnetic anisotropy and exchange interactions.

(Received July 1, 2025; Accepted October 23, 2025)

Keywords: Perovskite oxide, $NiMnO_3$, Co doping, Hydrothermal, Magnetic property

1. Introduction

Perovskite oxides with formula ABO_3, in which A is a rare or alkaline earth metal cation and B is a 3d transition metal cation, have attracted a lot of interest because of their exceptional redox characteristics, high oxygen storage capacity, thermal stability, and structural resilience at high temperatures [1,2,3]. These characteristics make perovskite materials suitable for a wide range of applications, including electrochemical sensors, metal-ion batteries, solar cells, fuel cells, and spintronic devices [4-9]. However, conventional synthesis methods such as sol–gel processes and solid-state reactions often result in perovskite oxides with low surface areas because of the high calcination temperatures (1073–1173 K) required, which lead to particle agglomeration. Among the various transition metal oxides, Ni/Mn-based oxides, particularly $NiMnO_3$, stand out due to their excellent physical and chemical properties, abundant resources, non-toxicity, and cost-effectiveness. $NiMnO_3$ has been thoroughly investigated for its potential in supercapacitors, water splitting, and electrocatalysis, and is also valued for its low dielectric properties, making it a promising material in the field of electromagnetic absorption [10-14]. $NiMnO_3$ material has also been potentially studied for its photocatalytic and photoluminescent properties [15,16]. In the vintage years, few researchers have observed the magnetic properties in $NiMnO_3$ and other

* Corresponding author: bslv85@gmail.com
https://doi.org/10.15251/JOR.2025.215.657

pervoskites such as $CoMnO_3$, $MgMnO_3$ and $AgMnO_3$ [17, 18]. The magnetic behavior of $NiMnO_3$ arises from the complex interactions between its constituent ions, primarily Ni^{2+} and Mn^{3+}, which occupy octahedral sites in the crystal lattice. These interactions can lead to various types of magnetic ordering, including antiferromagnetic, ferrimagnetic, or even canted antiferromagnetic arrangements, depending on the exact composition, temperature, and external magnetic field which can be exploited in several uses of technology, including magnetic sensors, data storage devices, and spintronics [19-21]. E. F. Bertaut et al, reported the ferrimagnetic nature in ilmenite type $MnNiO_3$ [22], also Cloud reported the same ferrimagnetic nature in $NiMnO_3$ and $CoMnO_3$ [18], however an antiferromagnetic nature has been observed in $MgMnO_3$ and $AgMnO_3$. The Curie temperature of $CoMnO_3$ and $NiMnO_3$ reported to be 391 K and 437 K respectively [23]. Hence, due to the different magnetic behaviour and interaction in $NiMnO_3$, motivated to study the optical and magnetic property of Co doped $NiMnO_3$. To our knowledge the magnetic property was not studied in the doped $NiMnO_3$. In the current work hydrothermal technique is used to prepare $NiMnO_3$, $NiMn_{0.95}Co_{0.05}O_3$ and $NiMn_{0.90}Co_{0.10}O_3$ nanoparticles, because it has several advantages over alternative methods, including scalability, affordability, ease of use, high purity, and uniformity. PXRD, UV-visible spectroscopy, PL and SEM were utilized to describe the prepared nanoparticles. The characterization results of the samples are very well suggested the Co doped $NiMnO_3$for various optical and magnetic device applications.

2. Materials and methods

The samples have been prepared through hydrothermal method. The metal precursor $Co(No_3)_2.6H_2O$, $Ni(No_3)_2.6H_2O$ and $Mn(No_3)_2.4H_2O$ have been taken with the required proportion and dissolved in 80 ml deionised water and stirred for one hour, then an alkaline solution of sodium hydroxide (NaOH) is added to the solution until pH reaches ~11, along with urea for hydrolysis. Next, the mixture is put in a teflon lined autoclave and heated to 140 °C for 12 hours. After the hydrothermal reaction, the resulting powder is washed thoroughly with ethanol and deionized water for several times to remove residual impurities and by products. After several hours, the dried sample is calcinated at 500 °C in muffle furnace for 4 hours. When the calcination process gets done, the samples were fine powdered using mortar and pestle. The phase cleanliness of the sample has been verified by the X-ray diffraction (XRD) method; the morphology of the sample is identified by scanning electron microscopy (SEM). The optical behaviour of the materials is studied through UV-Vis and photoluminescence spectroscopy.

Using X-ray photoelectron spectroscopy (XPS) technology, the surface chemical properties were investigated with Al K-alpha X-rays (Thermo Scientific, UK). Vibrating sample magnetometer (Lakeshore VSM 7410) was employed to calculate the field dependency of magnetization (M vs. H) at ambient temperature using a 2.5 T magnetic field.

3. Result and discussions

3.1. Powder XRD studies

The structural properties are ascertained using X-ray diffraction investigation utilizing the Philips PW 1729 system and Cu Kα radiation (CuKα=1.5418Å). The XRD spectra were used to evaluate the crystal structure of $NiMnO_3$, $NiMn_{0.95}Co_{0.05}O_3$ and $NiMn_{0.90}Co_{0.10}O_3$nanoparticles. Figure 1 depicts the XRD diffraction peaks of pure $NiMnO_3$ with the peaks observed at 25°, 34°, 37°, 42°, 51°, 55°, 64°, and 66°.

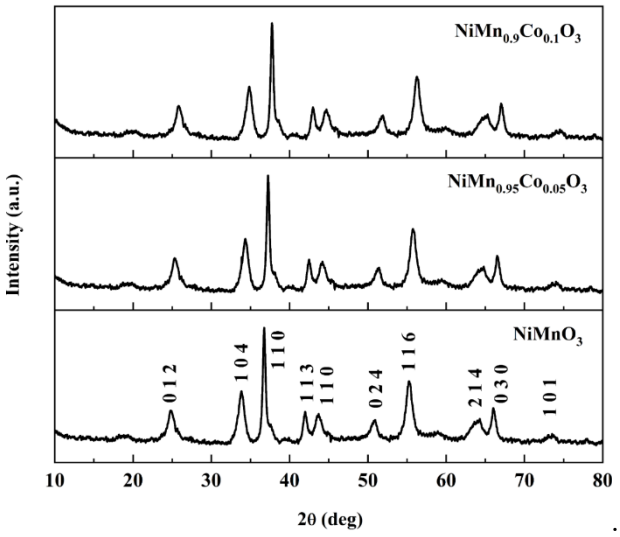

Fig. 1. PXRD spectrum of $NiMnO_3$, $NiMn_{0.95}Co_{0.05}O_3$ and $NiMn_{0.90}Co_{0.10}O_3$ nanoparticles.

These peaks correspond to the indexed crystal planes (012), (104), (110), (113), (024), (116), (214), and (300), respectively. For the XRD-indexed peaks, the JCPDS (#00–012-0269) with the space group R3-R provided excellent alignment. The XRD results shows that the $NiMnO_3$ are crystallized in rhombohedral structure as shown by the XRD diffractogram (Figure. 1). Similar XRD peaks has been reported in the Sm doped and Cu doped $NiMnO_3$ [24, 25]. The incorporation of Co^{2+} ions do not alter the fundamental rhombohedral structure of $NiMnO_3$, as no new peaks are observed in the XRD patterns. This indicates that Co is successfully integrated into the lattice without forming secondary phases. The peaks are substantially shifted to the higher angles, with the shift becoming more pronounced as the dopant concentration increased. This shift can be explained as the Co2+ ions typically have a smaller ionic radius (0.65 Å) compared to Mn2+ ions (0.83 Å). Hence the Co doping modifies the lattice dimensions while preserving the original crystal structure, demonstrating its potential for tuning the material's properties without disrupting the phase integrity. The particle size of the samples are calculated by Debye schrrer formula and found to be 19.9 nm, 20 nm and 20.9 nm for $NiMnO_3$, $NiMn_{0.95}Co_{0.05}O_3$ and $NiMn_{0.90}Co_{0.10}O_3$respectively. Hence the Co dopant increases the particle size.

3.2. UV – Visible spectroscopy analysis

The Perkin Elmer Lambda 950 spectrophotometer is used to measure optical characteristics in the UV-Vis region (200 nm to 800 nm). The absorption spectrum of the prepared nanoparticles is depicted in Figure. 2. One important parameter that can be obtained via UV-Vis spectroscopy is the material's bandgap. The least amount of energy needed to move a valence-band electron into the conduction-band is known as a bandgap [26]. The samples show a strong absorption around 500 nm, also the absorbance increases gradually at lower wave length and become broad at higher wavelength. However, in Mg doped $NiMnO_3$ the UV spectra at lower wavelength shows a broad absorbance in the visible region. The energy band gap of the materials was determined by Tauc's plot and shown in Figure 3. The obtained bandgap for $NiMnO_3$, $NiMn_{0.95}Co_{0.05}O_3$ and $NiMn_{0.90}Co_{0.10}O_3$ are 3.85 eV, 3.77 eV and 3.68 eV respectively. With the increase of Co ratio, the band gap value decreases and creates a path to easy electron transition from valence band to conduction band [27].

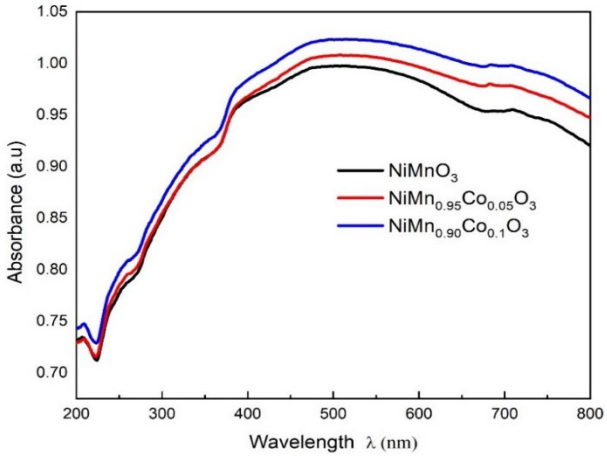

Fig. 2. UV- Visible absorption spectra of the synthesized nanoparticles.

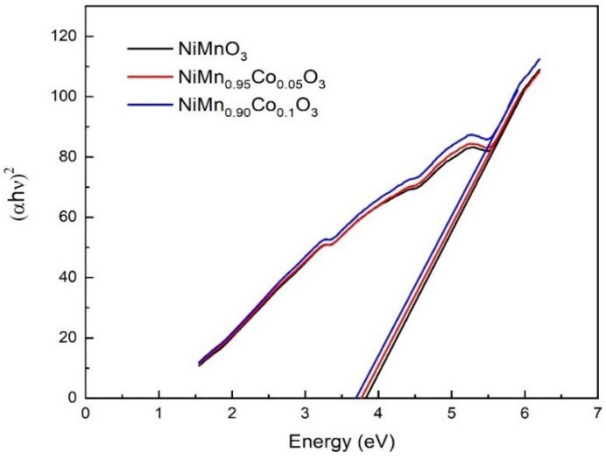

Fig. 3 Tauc's spectra of the prepared nanoparticles.

3.3. Photoluminescence studies

To study the luminescence characteristics, the samples are examined at room temperature with a Perkin Elmer LS 55 fluorescence spectrometer at an excitation wavelength of 350 nm. One key method that is able to understand us valuable information on the energy states of faults and impurities in semiconductors is PL spectroscopy [28].

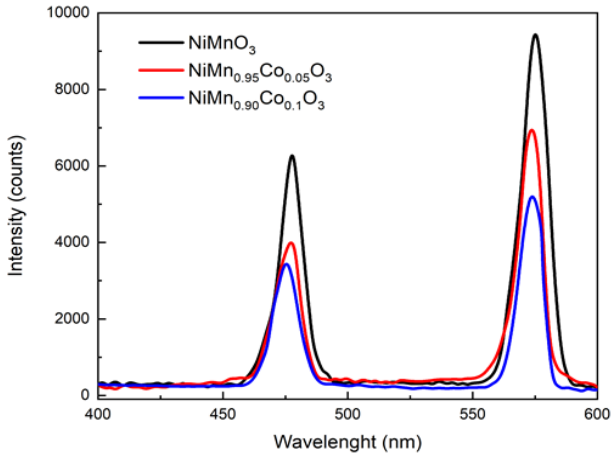

Fig. 4. Photoluminescence spectrum of the prepared nanoparticles.

Figure 4 illustrates the photoluminescence spectra of nanoparticles in the wavelength range of 400 to 600 nm. A blue emission peak occurs around 476 nm and another strong green emission peak occurs around 576 nm for all the samples ascribed to the near band edge and defect level emissions respectively. The reported Cu doped $NiMnO_3$ shows an emission only in blue region [25].

3.4. Scanning electron microscopy analysis

The SEM image of $NiMnO_3$ and Co doped $NiMnO_3$ is shown in figure 5. The $NiMnO_3$ sample shows as a big, slightly spherical or agglomerated structure at lower magnification. A porous or loosely packed structure is indicated by the surface's rough and grainy appearance. At reduced magnification, the $NiCo_{0.05}Mn_{0.95}O_3$sample has a massive, agglomerated structure, similar to the $NiMnO_3$ sample. Overall, the morphology looks similar, shaped fairly spherical. In comparison to the earlier samples, the $NiCo_{0.1}Mn_{0.9}O_3$sample exhibits a more fractured or uneven structure at lower magnification. The agglomeration is still there, but it may be less cohesive, suggesting that the increased level of Co doping has altered the microstructure of the material. The microstructure is easier to see in the photograph with increasing magnification. In comparison to the pure $NiMnO_3$ sample, the particles or grains seem more distinct, slightly smaller, or more evenly dispersed. For $NiCo_{0.1}Mn_{0.9}O_3$, the structure seems more porous or less densely packed at high magnetization; this could be because there are more flaws due to the increased Co content.

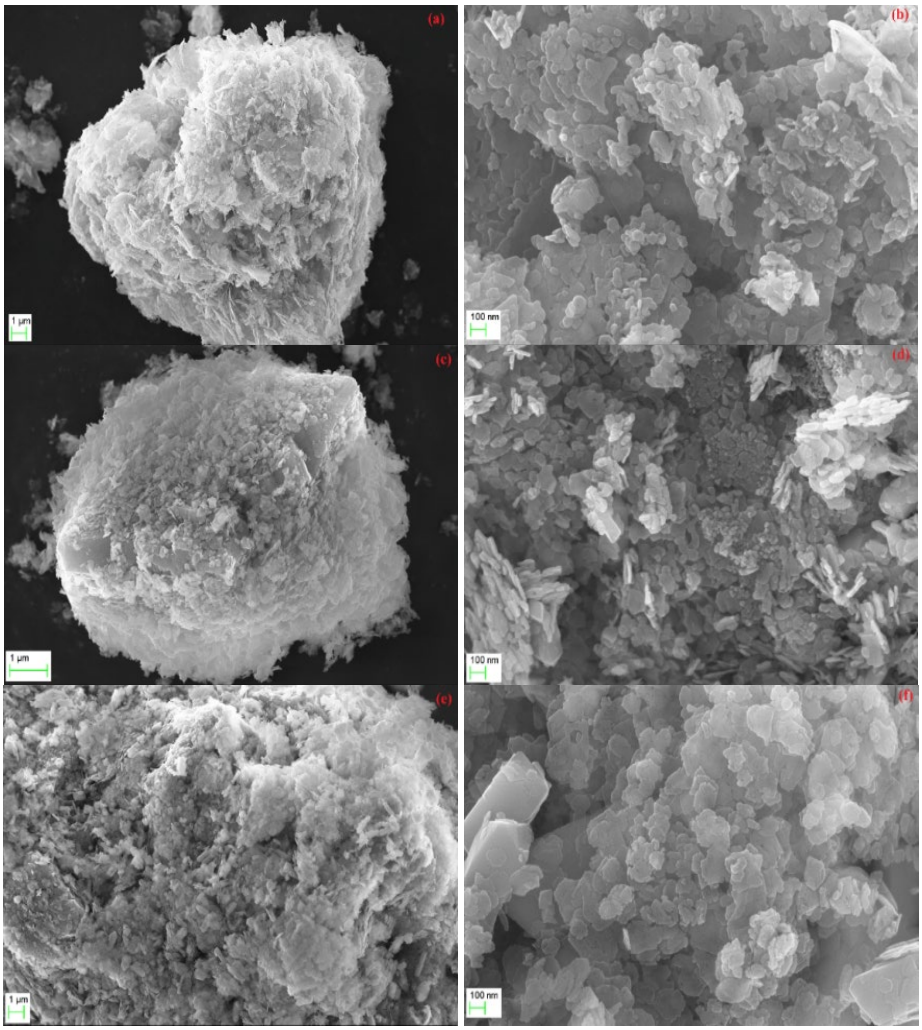

Fig. 5. SEM image of (a) and (b) $NiMnO_3$, (c) and (d) $NiCo_{0.05}Mn_{0.95}O_3$, (e) and (f) $NiCo_{0.1}Mn_{0.9}O_3$.

3.5 XPS study analysis

XPS analysis can provide chemical information such as oxidation state as well as the surface's semi-quantitative composition, enabling for the analysis of surface attributes. Figures 6 (a) shows the survey spectrum of $NiCoMnO_3$, indicates the presence of Ni 2p, Co 2p, Mn 2p, O 1s elements. The XPS high resolution deconvoluted spectra used to find oxidation plots of the elements. Figure 6 b shows the Ni 2p with peaks around 853.8 eV and 871.5 eV corresponds to state of $2p_{3/2}$ and $2p_{1/2}$ respectively [25]. The peaks around 860 and 878.5 eV corresponds to the satellite peaks of their respective Ni 2p. The binding energy of Co 2p were computed to be 779.6 and 795.5 eV which corresponds to $2p_{3/2}$ and $2p_{1/2}$ states of cobalt respectively which is shown in Figure 6 c. The satellite peak at 783.98 eV and an Auger peak at 774.6 eV has been observed for Co. The peak at 774.6 eV is caused by the particular Co LMM Auger transition that follows an initial core electron ejection and emits an Auger electron with this distinctive energy. Furthermore, the binding energy for Mn spin states were calculated to be 652.7 (Mn $2p_{1/2}$) and 641.2 eV and (Mn 2p3/2), respectively (Figure 6 d) [25, 29-30]. The XPS study confirms the clear synthesis of Co doped $NiMnO_3$ which is consistent with the XRD analysis.

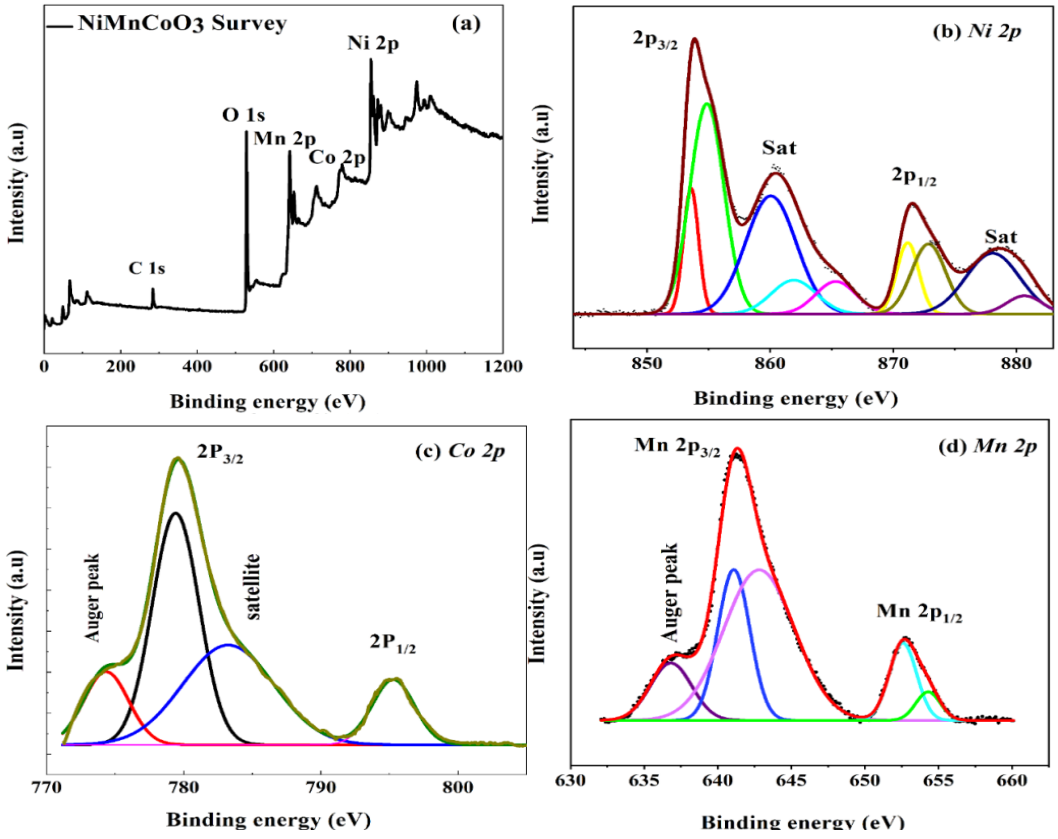

Fig. 6. XPS spectrum of Co doped $NiMnO_3$ (x = 0.1).

3.6. Magnetic study

The field dependence of magnetization (M-H) is measured for the $NiCo_xMn_{1-x}O_3$ (x = 0, 0.05, 0.1) sample with the field sweep of -2.5 T to 2.5 T at room temperature is shown in figure 7 (a, b & c). A week ferromagnetic ordering is observed in sample x = 0 and 0.05, and further doping of x = 0.1 leads to paramagnetic nature. Also, the overall magnetization value is reduced with doping of Co. As the Co content increases in the $NiCo_xMn_{1-x}O_3$ series, the material's magnetic properties shift from weakly ferromagnetic or ferrimagnetic, to paramagnetic behaviour. Most of reported, the magnetic nature of $NiMnO_3$ at room temperature is ferrimagnetic [17-18, 22-23].

Troyanchuk et.al., reported that the magnetic property depends on direct and indirect exchange interaction of Mn^{2+} and Ni^{2+} which results in ferromagnetic and antiferromagnetic nature respectively in $NiMnO_3$, whereas in $CoMnO_3$ the ferromagnetic and antiferromagnetic arises by indirect and direct interactions of Mn^{2+} and Co^{2+} [31]. Hence, in the present materials the weak ferromagnetic nature in $NiMnO_3$ arises because of direct exchange interaction, but for the higher Co dopant induces a paramagnetic nature. From the XPS and magnetic study it confirms that the Mn^{2+}, Co^{2+} and Ni^{2+} and their exchange interaction plays a major role in the formation of different magnetic behaviour in the present material. Hence in order to understand the present magnetic nature in Co doped $NiMnO_3$, the neutron diffraction analysis will be a good tool [32]. Further, the enlarged view of M vs H plot for all samples are shown in inset of their respective plot. The inset clearly indicates the coercive field present in the sample. The coercive field increased drastically with the increase of Co content and the observed coercive field are 1.5 Oe, 66 Oe and 90 Oe for x = 0, 0.05 and 0.1 respectively. In other terms the increase of particel size increases the coercive field of the materials.The increase in the coercive field with the doping of Co into Mn can be attributed to the combined effects of enhanced magnetic anisotropy and stronger exchange interactions which make the magnetic domains more stable and resistant to reorientation, thereby requiring a stronger external magnetic field to demagnetize or reorient the material, leading to a higher coercivity.

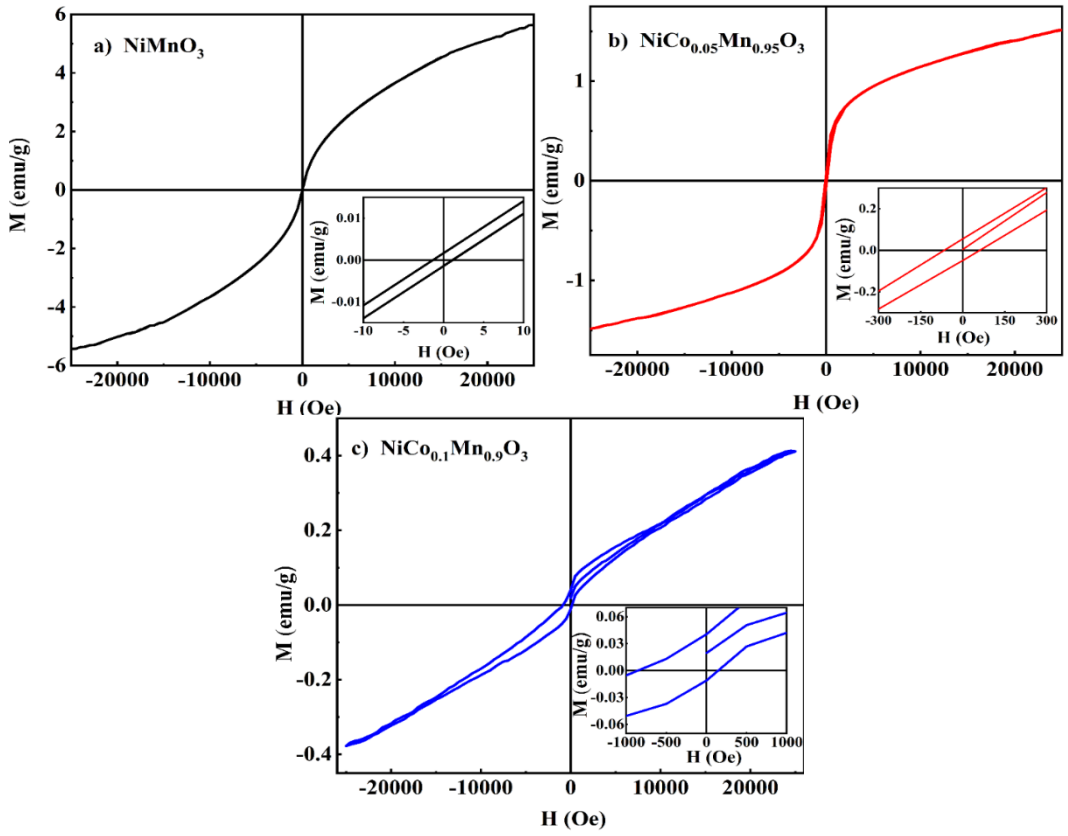

Fig. 7. Magneitc field dependance of (M - H) of Co doped $NiMnO_3$.

4. Conclusion

In conclusion, hydrothermal method was used to prepare $NiMnO_3$, $NiCo_{0.05}Mn_{0.95}O_3$ and $NiCo_{0.1}Mn_{0.9}O_3$ nanoparticles. X-ray diffraction measurements revealed that the crystal structure of nanoparticles is rhombohedral, and no alteration in the crystal's structure upon doping.The band

gaps of the nanoparticleswere determined using UV-Visible spectroscopy, and the band gaps were calculated as 3.85, 3.77, and 3.68 eV, respectively.The blue and green emission peaks in photoluminescence spectra are attributed to near band edge and defect level emission. Ultimately, we draw the conclusion that Ni replacements are crucial in lowering vacancy flaws. while magnetic measurements revealed a significant increase in coercive field, attributed to enhanced magnetic anisotropy and exchange interactions. These results underscore the potential of Co-doped $NiMnO_3$ nanoparticles for applications in optical and magnetic devices, where tuneable properties are desirable.

References

[1] C. Kim, O. Gwon, I. Jeon, Y. Kim, J. Shin, Y. Ju, J. Baek, G. Kim, J. Mater. Chem. 4, 2122-2127 (2016); https://doi.org/10.1039/C5TA08493H

[2] Y. H. Han, Korean J. Mater. Res. 2, 248-256 (1992).

[3] D. Bartolomeo, E. Kaabbuathong, N. D'Epifanio, A. Grilli, M.L. Traversa, E. Aono, H. Sadaoka, Y., J. Eur. Ceram. Soc. 24, 1187-1190 (2004); https://doi.org/10.1016/S0955-2219(03)00470-9

[4] N. Tsvetkov, B. C. Moon, J. Lee, J. K. Kang, ACS Appl. Energy Mater; https://doi.org/10.1021/acsaem.9b01592

[5] S. Tao, J. T. Irvine, Chem. Mater. 16, 4116-4121 (2014); https://doi.org/10.1021/cm049341s

[6] B. Yue, Q. Hu, L. Ji, Y. Wang, J. Liu, RSC Adv. 9, 38271-38279 (2019); https://doi.org/10.1039/C9RA07660C

[7] Jhelai sahadevan, M. Radhakrishnan, N. Padmanathan, S. Esakki Muthu, P.Sivaprakash, Mohanrangam Kadiresan, Materials Science and Engineering B 284, 115875 (2022); https://doi.org/10.1016/j.mseb.2022.115875

[8] B. B. Nelson-Cheeseman, R. V. Chopdekar, L. M. B. Alldredge, J. S. Bettinger, E. Arenholz, Y. Suzuki, Phys. Rev. B 76, 220410 (2007); https://doi.org/10.1103/PhysRevB.76.220410

[9] B. B.Nelson-Cheeseman, R. V. Chopdekar, J. M. Iwata, M. F. Toney, E. Arenholz, Y. Suzuki, Phys. Rev. B 82, 144419 (2010); https://doi.org/10.1103/PhysRevB.82.144419

[10] S. Qiao, N. Huang, Y. Zhang, J. Zhang, Z. Gao, S. Zhou, Int. J. Hydrog. Energy 44, 18351-18359 (2019); https://doi.org/10.1016/j.ijhydene.2019.05.108

[11] Y. Bu, S. Kim, O. Kwon, Q. Zhong, G. Kim, ChemElectroChem 6, 1520-1524 (2019); https://doi.org/10.1002/celc.201801775

[12] Y. Bu, H. Jang, O. Gwon, S. H. Kim, S. H. Joo, G. Nam, S. Kim, Y. Qin, Q. Zhong, S. K. Kwak, et al., J. Mater. Chem. A 7, 2048-2054 (2019); https://doi.org/10.1039/C8TA09919G

[13] S. Qiao, S. Zhou, N. Huang, J. Zhang, Y. Sun, L. Yang, X. Du, Mater. Lett. 255, 126509 (2019); https://doi.org/10.1016/j.matlet.2019.126509

[14] S. Qiao, N. Huang, J. Zhang, Y. Zhang, Y. Sun, Z. Gao, J. Solid State Electrochem. 23, 63-72 (2018); https://doi.org/10.1007/s10008-018-4115-8

[15] Muhammad Imtiaz, Rabia Yasmin Khosa, Lamia Abu El Maati, Salma Aman, Abdullah G. Al-Sehemi, A.M.A. Henaish, Taha Abdel Mohaymen Taha, Optik - International Journal for Light and Electron Optics 300, 171639 (2024); https://doi.org/10.1016/j.ijleo.2024.171639

[16] Shilpi Upadhyay, Insaaf Assadullah, Radha Tomar, Scientific Reports 14, 7415 (2024); https://doi.org/10.1038/s41598-024-52132-1

[17] B. L. Chamberlandt, A. W. Sleight, J. F. Weiher, Journal of Solid-State Chemistry 1,512-514 (1970); https://doi.org/10.1016/0022-4596(70)90134-9

[18] W. H. Cloud, Physical Review 111, 1046 (1958); https://doi.org/10.1103/PhysRev.111.1046

[19] Mukesh Kumar Verma, Narayan Dutt Sharma, Suman Sharma, Nisha Choudhary, Devinder Singh, Materials Research Bulletin, 125, 110813 (2020); https://doi.org/10.1016/j.materresbull.2020.110813

[20] Hua Wang, Shu-Ming Gao, Ji-Wen Xu, Chang-Lai Yuan, Xiao-Wen Zhang, Bull. Mater. Sci., 38, 105-109 (2015); https://doi.org/10.1007/s12034-014-0792-9

[21] R. Dong, W. F. Xiang, D. S. Lee, S. J. Oh, D. J. Seong, S. H. Heo, H. J. Choi, M. J. Kwon, M. Chang, M.Jo, M. Hasan, Hyunsang Hwang, Appl. Phys. Lett. 90, 182118 (2007); https://doi.org/10.1063/1.2736268

[22] E. F. Bertaut, F. Forrat, Journal of Applied Physics 29, 247-248 (1958); https://doi.org/10.1063/1.1723091

[23] T. J. Swoboda, R. C. Toole and J. D. Vaughan, J. Phys. Chem. Solids Pergamon Press 5, 293-298 (1958); https://doi.org/10.1016/0022-3697(58)90032-5

[24] S. Swathi, R. Yuvakkumar, G. Ravi, Abdullah G. Al-Sehemib, Dhayalan Velauthapillai, Rare earth metal (Sm)-doped NiMnO3 nanostructures for highly competent alkaline oxygen evolution reaction 4, 2501-2508 (2022); https://doi.org/10.1039/D2NA00022A

[25] Shilpi Upadhyay, Insaaf Assadullah, Radha Tomar, Scientific Reports 14, 7415 (2024); https://doi.org/10.1038/s41598-024-52132-1

[26] S.E.S. Monica, C.R. Dhas, R. Venkatesh, R. Sivakumar, R. Vignesh, V.A. Ferby J. Solid State Electrochem 26, 1271-1290 (2022); https://doi.org/10.1007/s10008-022-05159-1

[27] Muhammad Imtiaz, Rabia Yasmin Khosa, Lamia Abu El Maati, Salma Aman, Abdullah G. Al-Sehemi, A.M.A. Henaish, Taha Abdel Mohaymen Taha, Optik - International Journal for Light and Electron Optics 300, 171639 (2024); https://doi.org/10.1016/j.ijleo.2024.171639

[28] C. Mrabet, M. Ben Amor, A. Boukhachem, M. Amlouk, T. Manoubi, Ceramics International, 42, 5963-5978 (2016); https://doi.org/10.1016/j.ceramint.2015.12.144

[29] Y. Chen, L. T. Cao, P. Lian, J. H. Guan, Y. Liu, J. Alloys Compd. 832, 154936 (2020); https://doi.org/10.1016/j.jallcom.2020.154936

[30] M. Zhang, Electrochem. Acta 87, 546-553 (2013); https://doi.org/10.1016/j.electacta.2012.09.085

[31] I.O. Troyanchuk, A.A. Shemyakov, V.K. Prokopenko, Phys. Stat. Sol. (a) 113, K107 (1989); https://doi.org/10.1002/pssa.2211130151

[32] M. Pernet, J.C. Joubert, Etudepar Solid State Communications, 16, 503-508 (1975); https://doi.org/10.1016/0038-1098(75)90411-1